Tellus (2000), 52A, 42–65
Printed in UK. All rights reserved

TELLUS
ISSN 0280–6495

A numerical model comparison of baroclinic instability in the presence of topography

By CATHERINE GRIFFITHS*[1], MOTOYOSHI IKEDA[2] and PETER C. SMITH, *Bedford Institute of Oceanography, PO Box 1006, Dartmouth, Nova Scotia B2Y 4A2, Canada*

(Manuscript received 2 March 1998; in final form 4 June 1999)

ABSTRACT

The development of meanders along a front and subsequent eddy formation results in the exchange of water-mass properties across the front. This is an important phenomenon, both for continental shelf and basin-scale thermodynamics. In this study, we are concerned with the authenticity of growing baroclinic waves over bottom slope topography in commonly-used primitive equation models, as they are such a widely used tool for understanding the dynamics of the ocean. Baroclinic instability is simulated in a cyclic channel, in 2 such models: the Bryan–Cox model (Cox, 1984) and the Bleck–Boudra (1986) isopycnal model. We focus on the linear stage of instability and on the effects of topography, with isobaths running parallel to the front. Initially, a quasi-geostrophic (QG), subsurface front is used as a basic state for baroclinic instability in the 2 models. A series of experiments with topography are performed, introducing successively steeper topography parallel to the front. The results from the 2 models are verified by comparison with QG theory and results from a QG numerical simulation. Two versions of the isopycnal model, which employ different numerical schemes for advection in the thickness equation, are run for the flat-bottomed experiments. We demonstrate how this choice of numerical scheme can affect baroclinic wave activity. Linear growth rate curves are plotted for each model experiment. The fastest-growing baroclinic wave in a flat channel is shorter in the Bryan-Cox model than that predicted by QG theory, QG numerical model results, and the Bleck–Boudra isopycnal primitive equation model. This feature is a consequence of the vertical discretization used in this model. The magnitude of the linear growth rates is significantly smaller in the Bleck–Boudra isopycnal model than in the Bryan–Cox model and the QG simulation, because of implicit diffusion inherent in the numerical scheme used by this model. The experiments with topography show that this implicit diffusion becomes most active in more stable environments. The modifying effects of topography expected from QG results are found in both primitive equation models: for topography of positive slope (i.e., with the same inclination as the isopycnals), the fastest-growing wavelength increases and is damped; for topography of negative slope, the fastest-growing wavelength decreases. The 2 primitive equation models are then initialized with an ageostrophic, outcropping front; and their results are compared in the light of experience gained from the subsurface front simulations. Again, a series of experiments with topography are performed. The results from these simulations show how ageostrophic effects act to stabilize baroclinic waves, but do not change the way that topography modifies them. Similar, numerically-induced, features were found in all the experiments with the ageostrophic, outcropping front, as was found with the subsurface front. By focusing on the linear growth of baroclinic waves, this investigation has pinpointed some artificial tendencies inherent in the 2 primitive equation models, which modellers will find useful when interpreting the results of their simulations. The

* Corresponding author.
Present affiliations: [1]Department of Mathematics, North Park Road, Exeter, Devon EX4 4QE, UK.
e-mail: cathy@maths.ex.ac.uk [2]Graduate School of Environmental Earth Science, Hokkaido University, North 10 West 5, Kita-ku, Sapporo, Japan 065.

important lesson for oceanographers is to remember, that although waves in the numerical models are physically well-behaved, the wave characteristics may have been modified by numerical errors, and therefore to exercise care in interpretating the results.

1. Introduction

Baroclinic waves play a dominant rôle in transporting momentum, heat, salt and biological tracers within the ocean. The transport of these quantities between continental shelves and their offshore basins is critical to the understanding, and simulation of, the formation of various types of water masses and biochemical product distributions, in both the shelf areas and the basins. A couple of examples are the cold halocline water in the Arctic Basin, and sea–ice cover over the Labrador shelf. In order to estimate the shelf-basin exchanges, it is necessary to understand the dynamic processes of fronts, and their associated currents, over shelf-slope topography. A logical, widely used tool, for this purpose is a primitive equation (PE) model. PE models retain appropriate physics, but have shortcomings under any particular model configuration, because of their mathematical and numerical complexity.

Numerical models have been successfully reproducing the gross features of the ocean for some years. Nevertheless, some of the finer details of the currents seem to be particularly difficult for the models to get right (Wang, 1997; Roberts et al., 1996; Wilkin et al., 1995; Chassignet, 1992). There are 2 possible reasons why the models are unable to reproduce reality: either a relevant physical process has been neglected in the analytical development of the model, or numerical errors associated with the discretization process of the models are modifying the solution. Here, we focus on the latter possibility, and investigate how the vertical discretization of PE models can affect the simulation of baroclinic waves. Numerical analysis can establish convergence, error bounds and tendencies of numerical schemes for simplified equations (invariably 1-dimensional). However, careful numerical testing still needs to be done for more complex sets of equations (i.e., PE models), as non-linearities and feedbacks between the equations can amplify numerical errors and change the behaviour of the solution. This field of investigation is relatively new, since it is only recently that both the necessary hardware and software have become available to the oceanographic community (Hecht et al., 1995; Hecht et al., 1998). It is an area which must be fully examined before oceanographic modellers will be in a position to predict oceanic phenomena accurately.

PE models are best verified with a simpler model, whose behaviour is well understood, rather than comparison with data. Drijfhout (1992) has compared the characteristics of Gulf-Stream-like meanders in 3 numerical models: a quasi-geostrophic (QG) model; a z-coordinate model based on the numerical techniques developed by Bryan (1969); and an isopycnal model (Bleck and Boudra, 1986). He focused on the characteristics of a fully developed baroclinic wave, that is, the non-linear stage. The lifetime of the wave was prolonged in the z-coordinate model compared to the others, which was attributed to spurious diapycnal diffusion. Heat fluxes associated with the baroclinic wave were found to be quite sensitive to the horizontal resolution in the z-coordinate model. This was not the case with the isopycnal model.

In an analytical approach, Ikeda and Wood (1993) looked at how vertical discretization can alter the linear stability properties of purely baroclinic waves in primitive equation models. They found the maximum growth rate of baroclinic waves in the Bryan (1969) type model to be overestimated and to occur at too short a wavelength, with poor vertical resolution. However, when the vertical resolution is increased, a spurious short wave instability appears, whose existence is a consequence of the way in which the variables are discretized in the vertical. They also demonstrated that these problems do not arise in layer models (for example, an isopycnal model). Numerical experiments (Wood and Ikeda, 1994) showed that the growth rate curve of a QG baroclinic wave in the Bryan (1969) type model did converge towards the QG results as the vertical resolution was increased. However, the vertical resolution had to be extremely fine before the maximum growth rate occurred at the correct wavelength. This paper was concerned with the differences found between a QG and a PE model's simulation of baroclinic wave growth along a subsurface front. They explored the range of 2 parameters in the PE model: the vertical resolution, and the strength of the current (using a stratification based on the Norwegian Coastal Current). All of their experiments were in a flat-bottomed, cyclic channel.

Numerical studies of ageostrophic fronts overlying bottom topography have been done (Chao, 1990; Maskell et al., 1992). The stratification of each ageostrophic front can be critical in determining the instability of the front and how bottom topography will modify it. Maskell et al. (1992) used a primitive equation model (Cox, 1984) to study how a number of different steep topographic profiles modified the development and structure of baroclinic instabilities along an outcropping ageostrophic front, in the absence of external forcing. Their choice of stratification and topographic slope was based on that of the Iceland-Faerœ front. Chao (1984) simulated baroclinic instability in a cyclic channel with a steep continental shelf by diffusing saltier or fresher water into the model over the shelf region. Strong and weak fronts were created, sloping in the same sense as the topography and opposing it, by varying the buoyancy flux and the initial stratification. He analysed the resulting instabilities in terms of how large they grew and whether cyclonic or anticyclonic motions dominated. There is still much work to be done in this rather large area of research. Here we present a numerical model comparison of the linear growth of baroclinic waves in the presence of bottom slope topography, most of which can be verified with QG theoretical results.

The strategy we adopt is to investigate the ability of 2 PE models in reproducing the linear stages of baroclinic instability over bottom slope topography. Accurate simulation of baroclinic instability is fundamental to the development of realistic models of the ocean, as they play such an important rôle in the thermodynamics of ocean. In addition, the linear growth of such waves is well understood, which makes this phenomena ideal for a careful numerical investigation. The authenticity of a baroclinic wave or eddy in its well-developed stage is difficult to evaluate, since there is neither theory nor sufficient observations to validate the model results. For this reason, we do not attempt to assess the non linear stage of the instabilities in the models. Nevertheless, it is clear that unless the initial growth is accurately reproduced, there is little chance that subsequent, finite amplitude, development will be realistic.

The PE models chosen for this investigation have philosophically different vertical discretizations: a z-coordinate model (Cox, 1984) and an isopycnal model (Bleck and Boudra, 1986). In a frontal region where pycnocline depths change dramatically, and in regions where topography plays an important rôle, the representation of stratification is likely to have important implications on the way that potential vorticity and other quantities move around within the fluid.

In this type of investigation, it is important to remember that each numerical model has its pros and cons, and performs best under specific circumstances. To a large degree, the physical situation which the model attempts to reproduce determines how well the model behaves. For example, if a model performs well in a coarse-resolution global oceanic simulation, we cannot necessarily extrapolate this result to a fine-resolution coastal simulation. It is therefore important to clarify the approach of this investigation.

We conduct our experiments with fine horizontal resolution, and therefore we do not address the question of horizontal resolution, or eddy parameterization in coarse-resolution model simulations. Although there are many parameters one could explore; one must keep focused in order to make any deductions. In terms of the numerics, we chose to compare simulations from two, numerically different, PE models. In terms of the physics, we chose to study the effect of bottom slope on growing baroclinic waves.

Baroclinic instability is simulated in a cyclic channel using 2 different fronts as a basic state: a gentle subsurface (QG) front, and a steeper (ageostrophic) outcropping front. In both cases, we vary the across-channel bottom slope in order to look at the effects of topography. Each oceanic front has a unique character, based on the water masses involved and any associated topography. We use the Labrador Current front as a basis for making choices about the stratification and topography in our numerical simulations. Since our primary aim is to perform a careful numerical model evaluation, we limit our experiments to a simplified model setup, rather than attempting a realistic simulation (with complex geometry, complex topography, external forcing, etc.) which would be difficult, if not impossible, to verify.

The approach taken here is to examine how the representation of topography in the numerical models modifies the growth of baroclinic waves. With this in mind, we take a step by step approach: first simulating the growth of baroclinic waves in a flat-bottomed channel; and then introducing progressively steeper topography into the channel. The introduction of bottom topography into finite difference models is not a straightforward matter because of the discrete nature of the models. Both of the PE models used here have undergone the commonly used test of examining the behaviour of a barotropic current impinging on a seamount (Huppert and Bryan, 1976; Smith, 1992). Frontal interaction with topographic features is not generally used as a test for numerical models, because of the difficulties involved in verifying the results.

First, we establish the properties of the waves (by a careful examination of the energetics and growth rates) which develop along a gentle, QG, subsurface front in the 2 models with no topography. Linear growth rate curves are plotted for each model. Such plots show both the temporal and spatial scales of the waves, which develop along the front undergoing instability. The PE model results are then verified by comparison to linear QG theory of baroclinic instability and a QG numerical model simulation. Once the flat case has been analysed, we incorporate topography into the models and observe how this modifies the growth rates in each model. This can again be compared to theoretical and numerical QG model results. Having established the model characteristics of wave growth along a gentle subsurface front over bottom slope topography, the study proceeds by initializing the models with a steeper (ageostrophic) outcropping front, and then by incorporating progressively steeper topography into that model setup.

The main questions addressed here are: (i) How well do the 2 primitive equation models reproduce the linear stage of baroclinic instability? (ii) How do the models differ in their simulations? (iii) How does topography modify the characteristics of the unstable waves in these models? (iv) Are the features found in the simulations of QG baroclinic instability replicated with the ageostrophic, outcropping front?

Section 2 describes the models which are used and the experiment design. The subsurface front experiments are documented in Section 3, and the outcropping front experiments in Section 4. The results are summarized in the final section.

2. Model descriptions and experiment design

We examine the baroclinic instability process in 2 primitive equation models: the Bryan–Cox model (Cox, 1984) and Bleck and Boudra's (1986) isopycnal model, henceforth referred to as the BC and BB models respectively. The primary difference between these 2 models is the vertical coordinate they use, which has repercussions on the way that topography is represented, and on the vertical resolution of fronts, jets, and eddies. The relevant characteristics of these models are summarized below. Full details of the models can be found in the references mentioned above.

2.1. Bryan–Cox model (BC)

Although the development of the code is attributed to Cox (1984), we refer to this model as the Bryan–Cox (BC) model, since the methodology was based on the numerical methods developed by Bryan (1969). This primitive equation model has been the most widely used by the deep sea oceanographic community. It was originally developed for ocean scale simulations (Cox and Bryan, 1984), but has proved to work reasonably well for finer resolution studies.

BC is a z-coordinate model, written in spherical coordinates, with predictive equations for both temperature and salinity. The density is determined from Knudsen's equation of state (Fofonoff, 1962). The numerical formulation of the model is such that the barotropic (depth independent) and baroclinic components of the flow are calculated separately (Bryan, 1969). Since the barotropic velocity field is 2-dimensional, a barotropic streamfunction, ψ, can be defined. This variable is used as a dependent variable instead of pressure. A predictive equation for the streamfunction is found by taking the curl of the vertically averaged zonal and meridional momentum equations. This equation is solved iteratively (Cox, 1984). The boundary conditions used in the model are: a rigid lid at the upper boundary; no slip conditions for the horizontal velocities, both laterally and at the bottom; and no heat or salt fluxes through any of the boundaries.

The numerical characteristics of this model, described in detail in Bryan (1969) and Cox (1984), are summarized here. It is discretized on an Arakawa B-grid, and uses the leap-frog time scheme for all terms apart from the Coriolis and diffusion terms. The Coriolis terms are treated semi-implicitly, and an Euler forward scheme is used for the diffusion terms. The Matsuno scheme (Matsuno, 1966) is implemented every 10 timesteps to prevent the 2 leap-frog solutions from diverging. The model conserves momentum, density, and energy, in the absence of dissipation.

In this model topography is represented by steps, the drop in each step being determined by the horizontal and vertical resolution chosen. In regions of steep topography, insufficient vertical resolution can cause problems with the velocity fields (Killworth, 1987; Killworth et al., 1991). For the experiments described here, we chose the finest resolution to be in the upper 300 m where the front is located, and at the bottom of the channel where topography will be introduced.

A timestep of 30 min was used. The coefficients of horizontal and vertical diffusion of momentum were chosen to be 5×10^5 cm^2 s^{-1} and 1 cm^2 s^{-1} respectively; and the coefficients of horizontal and vertical diffusion of temperature and salt 1×10^5 cm^2 s^{-1} and 1 cm^2 s^{-1} respectively. In this model diffusion occurs primarily along horizontal surfaces, which is not particularly desirable from a physical viewpoint. Drijfhout (1992) argues that this phenomenon has a significant effect on the character of the fully developed waves generated in this model.

2.2. *Bleck and Boudra model (BB)*

In this model, the vertical coordinate used is density, ρ, and hence it is called an isopycnal model. The coordinates are called material surfaces, since in an incompressible fluid, $D\rho/Dt = 0$, and the fluid particles move along density surfaces. The main advantages of this coordinate system are: (i) the diffusion of momentum occurs along density surfaces, which is more pleasing from a physical viewpoint; and (ii) fewer layers are needed to resolve a deep ocean with frontal regions, since high vertical resolution in the model is coincident with strong stratification. It is a rigid-lid model solved on a β plane. Temperature and salinity are not considered as independent entities in this model; only isopycnal layer thickness, $\partial p/\partial \rho$, is predicted.

In order to satisfy the rigid lid boundary condition, the flux form of the momentum equations are integrated over the water column, which results in a Poisson equation for the divergent component of the flow (see Appendix D in Bleck and Boudra, 1981). This equation is solved for the divergent component of the velocity field, which is then subtracted from the total velocity field (found by integrating the momentum equations), thereby ensuring that the rigid-lid condition is satisfied. Details of this model can be found in Bleck and Boudra (1986). We will henceforth refer to this model as the BB model. It is solved on a C-grid, and uses the leap-frog time scheme. An Asselin time filter (Asselin, 1972) is used to prevent the 2 leap-frog solutions from diverging.

Two versions of the isopycnal model are used. These will be referred to as "centred" and "FCT". The "centred" version uses a centred scheme for the advection terms in the thickness equation (i.e., the equation predicting layer thickness, $\partial p/\partial \rho$) and employs a direct method using FFT routines to solve the Poisson equation alluded to above. This version of the code has free slip boundary conditions, both laterally and at the bottom, and conserves enstrophy. The "FCT" version uses the flux corrected transport scheme (Zalesak, 1979) for the advection terms in the thickness equation; and solves the Poisson equation iteratively, using successive over-relaxation. The flux corrected transport (FCT) scheme is a positive definite advection scheme. Employing the FCT scheme for the nonlinear terms in the thickness equation allows layer thicknesses to become zero, so that isopycnals are able to intersect the sea bed or the sea surface. This version does not conserve energy or enstrophy, since these cannot be conserved in the outcropping regions. Nevertheless, these quantities will be conserved in a gross sense on the timescales considered here. The lateral boundary conditions are no slip, and there is no bottom friction in the FCT version of the model.

The timestep used was 10 min, and the isopycnal viscosity coefficient was chosen to be 5×10^5

$cm^2 s^{-1}$. There is no density diffusion in this model, which is desirable for adiabatic processes.

Problems associated with this coordinate system arise when diabatic effects become important. Experiments with topography so far (Smith, 1992) indicate that this model is well-behaved when topography is encountered by a barotropic current. Here, we look at this issue from another perspective: baroclinic instability over a topographic slope. Investigating the behaviour of a baroclinic current in the presence of topography, as is done here, is perhaps the most difficult test for a numerical model.

This coordinate system is relatively new to the oceanographic community, but is becoming more popular as the numerical difficulties associated with diabatic effects have been overcome (Bleck and Smith, 1990; Oberhuber, 1993; New et al., 1995).

2.3. Experiment design

The instability of a front in a channel with cyclic boundary conditions is the setup used to compare the models. The depth of the channel is 1 km, the width is 100 km, and the length of the channel varies as we simulate the instability of different wavelengths. The horizontal grid size is 5.559 km, although this varies slightly between the models since the map projections used are different. (The channel width and lengths referred to in this paper are rounded-off numbers.) For practical reasons associated with the numerical codes, the front and the channel are aligned east–west in this study. Since the planetary β effects are minimal over the length scales under study here, the orientation of the channel plays no important rôle. Laplacian friction is used in both models and Laplacian diffusion is used in the BC model. No external forcing is applied to the models.

First, we look at the stability properties of a geostrophically balanced, subsurface front, which satisfies the QG assumption that isopycnal depth variation is small compared to the thickness of isopycnal layers. The structure of this front is described in Section 3. We chose such a scenario so that we could use both analytical and numerical QG results as a reference solution for the primitive equation models. Both analytical and numerical QG solutions have their advantages: the theory provides mathematical purity, whilst the numerical results are able to employ the identical initial and boundary conditions that were used for the primitive equation models. Details of the QG numerical model we used for this purpose is documented in Ikeda (1981). Henceforth we refer to this model as the QG model.

The primitive equation models are run for several weeks and the linear growth rate of the frontal instability which develops is determined using the methodology described in Subsection 3.2. The length of the channel is then varied, and again the linear growth rates are noted. In this way, plots of growth rate against wavenumber (i.e., growth rate curves) are produced, which serve as a quantitative tool, both for verification with QG results and primitive equation model comparison.

Then topography is introduced to the models and the experiments are repeated. The topography varies only across the channel, in order not to excite wavelengths which may be at odds with the cyclic boundary conditions. The channel depth beneath the front is kept at 1000 m, with a constant topographic gradient across the channel. We look at 2 orientations of the topography: with the seabed sloping in the same sense as the isopycnals and with the seabed sloping in the opposite direction (see Fig. 1). These 2 slopes will be referred to as positive and negative slopes respectively. We perform a series of experiments for both orientations of topography, gradually increasing the

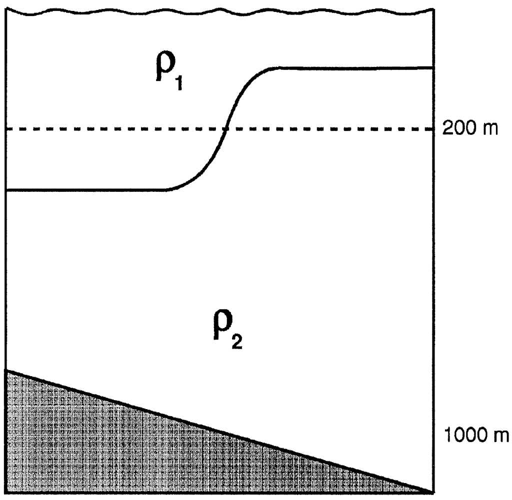

Fig. 1. Across-channel section of the subsurface geostrophic front with negative topographic slope.

gradient. For each slope, baroclinic instability is simulated for a number of channel lengths, so that growth rate curves can be produced.

Once the stability properties of a subsurface front in the 2 primitive equation models has been established we move on to simulate the instability of an (ageostrophic) outcropping front, in both models. Details of the structure of this front are described in Section 4. Experiments were performed for the flat channel and the negative orientation of topography. In a similar way, growth rate curves were plotted for this front, and used as the primary tool for model comparison.

3. QG subsurface front instabilities

The initial profile of the front is represented by 2 layers of constant density. The depth of the upper layer, $h(y)$, is of the form:

$$h(y) = H_o - \frac{U_o f}{g'} \int_{y_o}^{y} \exp\left\{ -\left(\frac{y - y_o}{a}\right)^2 \right\} \mathrm{d}y, \tag{1}$$

where y is the across-channel independent coordinate, y_o is the location of the front, H_o is the mean depth of the upper layer, U_o is the maximum speed of the current associated with the front, f is the Coriolis parameter, $g' = g(\rho_2 - \rho_1)/\rho_2$ is reduced gravity, ρ_1 and ρ_2 are the densities of the upper and lower layers respectively, and a is the width of the front. The initial potential vorticity is constant within each isopycnal layer. In the BC model, the transition between the 2 layers occurs over several z-levels, and it is here that variations in potential vorticity are found. The geostrophic current associated with this front is:

$$u(y) = U_o \left(1 - \exp\left[-\left(\frac{y - y_o}{a}\right)^2 \right] \right). \tag{2}$$

We chose $H_o = 200$ m, y_o to be the centre of the channel, $U_o = 30$ cms^{-1}, $\rho_1 = 1.02669$ g cm^{-3}, $\rho_2 = 1.02775$ g cm^{-3}, and $a = 1.8$; $R_d = 28.86$ km, where $R_d = \sqrt{g' H_o (H - H_o)/H f_o^2} = 12.698$ km is the internal Rossby radius and H is the total depth of the fluid. The densities were chosen to be representative of the Labrador Current. The profile of this front is illustrated in Fig. 1.

The initial density field is disturbed in the upper 220 m, with a sinusoidal perturbation having a wavelength the same as the channel length, L_x. (The initial geostrophic velocities are in balance with this disturbance.) The amplitude of the perturbation is 1°C and 0.1‰ salinity in the BC (level) model and a 1 m interface displacement in the layer models (that is, the BB and QG models). The form of the perturbation is:

$$\sin\left(\frac{2\pi x}{L_x}\right) \exp\left\{ -\left(\frac{y - y_o}{a}\right)^2 \right\}.$$

The introduction of a perturbation speeds up the development of the meander, which would otherwise take an inordinately long time to grow. The reader is reminded that only waves having a wavenumber which is a multiple of $2\pi/L_x$ are able to grow in this configuration, because of the cyclic boundary conditions. The disturbance having a wavelength L_x is given a head start by the introduction of the perturbation. It is almost always this wave which is seen to grow. The only situation when this does not occur is in fairly long channels, when the growth rate of the $L_x/2$ wave is significantly larger than the L_x wave, in which case the former develops.

In the BC model, 20 levels were chosen to represent the water column. Going down the water column, the layer thicknesses were chosen to be: 2×40 m, 6×35 m, 1×40 m, 6×70 m, and 5×50 m. In the runs with topography, the number of levels used is increased, so that the maximum depth in the centre of the channel remains 1000 m. Additional levels are added of thickness 50 m. In the QG and BB models, only 2 isopycnal layers were required to represent the subsurface front.

As an indication of the computational expense of the models, we compare the CPU time needed to run the primitive equation models with that required to run the QG model. For these experiments with the subsurface front in a flat channel, the BC model took 57× as long to run as the QG model did; the "centred" version of the BB model took 34× as long to run as the QG model; whilst the "FCT" version of the BB model took 264× as long.

3.1. *Meander development*

The models were initialized with the subsurface front described above, and integrated for a 40 day period (or in some cases a bit longer). The development of a typical meander is now shown for the BC model. Fig. 2 shows the potential vorticity at

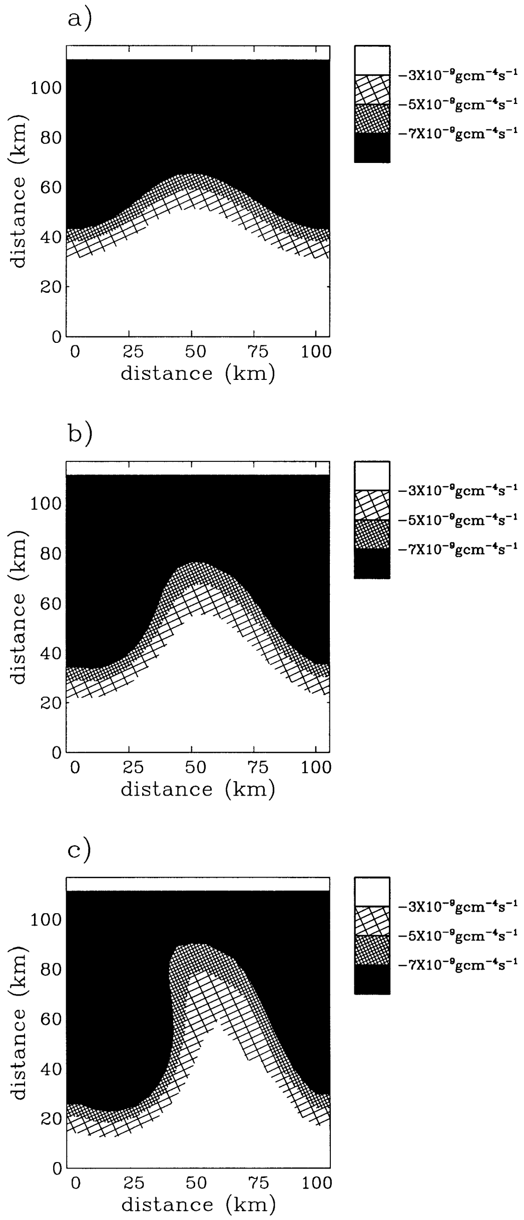

Fig. 2. The potential vorticity at 167 m depth for the 100 km length flat channel in the BC model: (a) 25, (b) 29, and (c) 33 days after initialization.

167 m for the 100 km channel length with no topography, at days 25, 29 and 33, respectively. Potential vorticity (defined by $(\xi + f)\,\partial\rho/\partial z$, where ξ is the relative vorticity) is always a negative quantity, since $\partial\rho/\partial z < 0$. At 167 m, the upper layer fluid is encountered in the southern half of the channel, and the highly stratified water (found at the interface of the 2 layers) is present in the northern half of the channel (cf. Fig. 1). The homogeneous pool of water in the south corresponds to low (negative) values of potential vorticity, whilst the highly stratified water in the north corresponds to high (negative) values of potential vorticity. The time sequence shows a typical example of meander development in the models: the perturbation developing into a meander somewhere between 15 and 20 days after initialization, with fairly rapid growth occurring once the meander has become established. The disturbance is seen to move along the front, advected by the mean current. It can be seen in Fig. 2 that throughout the linear stage of growth, the meander, with its associated density anomalies and velocities, is confined to the centre of the channel, and is therefore unaffected by the channel walls. Experiments performed with wider channels confirmed that the walls do not affect the results presented here.

If we are to compare the results of these models with QG baroclinic instability theory, we want to be sure that the meanders observed in the models are baroclinic waves. This was established by an analysis of the energetics in the BC model. The fields were decomposed into an along-channel average and deviations from this field, henceforth referred to as mean and eddy fields respectively. The energy is partitioned into 3 components: potential energy, PE; mean kinetic energy, MKE; and eddy kinetic energy, EKE. Interchanges between these 3 forms of energy were calculated at every timestep during the model integrations. This type of energy analysis is similar to that carried out by Orlanski and Cox (1973). For mathematical details of the energy conversion terms, the reader is referred to Griffiths (1992). The 3 terms responsible for regulating the amount of EKE in the system are plotted as a function of time in Fig. 3, from the 100 km length, flat-channel run. The 3 terms plotted are: (i) the baroclinic conversion term (conversion of PE into EKE); (ii) the barotropic conversion term (conversion of MKE into EKE); (iii) the dissipation of EKE.

This figure shows that these waves are certainly baroclinic: they extract PE from the system and convert it into EKE. For the example shown,

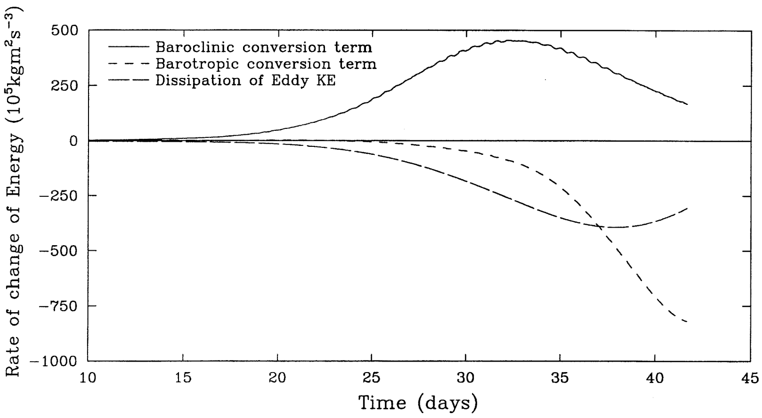

Fig. 3. A time series of the 3 terms responsible for regulating the amount of eddy kinetic energy in the 100 km length flat-channel run with the BC model.

meander growth starts around day 18. The shorter the wave, the shorter was the time interval between initialization and meander growth. As the wave grows, the dissipation of EKE increases; always acting to retard the growth of the wave. The barotropic conversion term comes into play once the wave has reached its maximum amplitude (seen in this figure as the maximum in the baroclinic conversion term). It plays a significant rôle in the decay of the wave: transferring energy from EKE to MKE via the Reynolds stresses. This term dominates the regulation of EKE in the decay stages of the wave. The energetics presented here conforms with classical baroclinic wave theory (Lorenz, 1967; Orlanski and Cox, 1973; Ikeda, 1981).

3.2. *Flat-channel case*

The subsurface front which provides the basic state for these model experiments allows us to compare the growth rates of the baroclinic waves in the primitive equation models with those predicted by theoretical and numerical QG models. The stability analysis incorporating the effects of topography for a purely baroclinic current is shown in the appendix for the reader's reference. We also derived the dispersion relation for a current with a Gaussian structure, using numerical integration to solve the eigenvalue problem. Since the growth rate curves were very similar, we only present the simpler solution here. The QG numerical model was run with cyclic boundary conditions, and the same channel dimensions and initial thermodynamic fields that were used for the 2 primitive equations models. By its nature a numerical QG model is a mathematically simplified layer model, giving little source for numerically induced errors. Indeed, the linear growth of baroclinic waves along the subsurface front simulated by the QG model replicates that predicted by QG theory.

The kinetic energy of each model run was partitioned into an along-channel mean, $\overline{KE}$, and deviations from this mean, KE'. When the front becomes unstable, the growth rate of the meander was determined from the quantity

$$\frac{1}{2}\frac{\partial(\ln\{KE'\})}{\partial t},$$

where

$$KE' = \frac{1}{2}\sum_{ijk}(u'^2 + v'^2)\,\mathrm{d}v,$$

and (u', v') is the deviation of the velocity field from the along-channel average, and the indices i, j, and k refer to the 3 spatial dimensions of the model. (The factor of a half makes this equivalent to the growth rate of the velocity field.) This quantity was calculated at every timestep in the model calculations. Linear growth of a single baroclinic wave will retain its shape and structure as it grows in amplitude. For linear wave growth, analytical solutions are invariably found by assuming such development: that is, the shape of

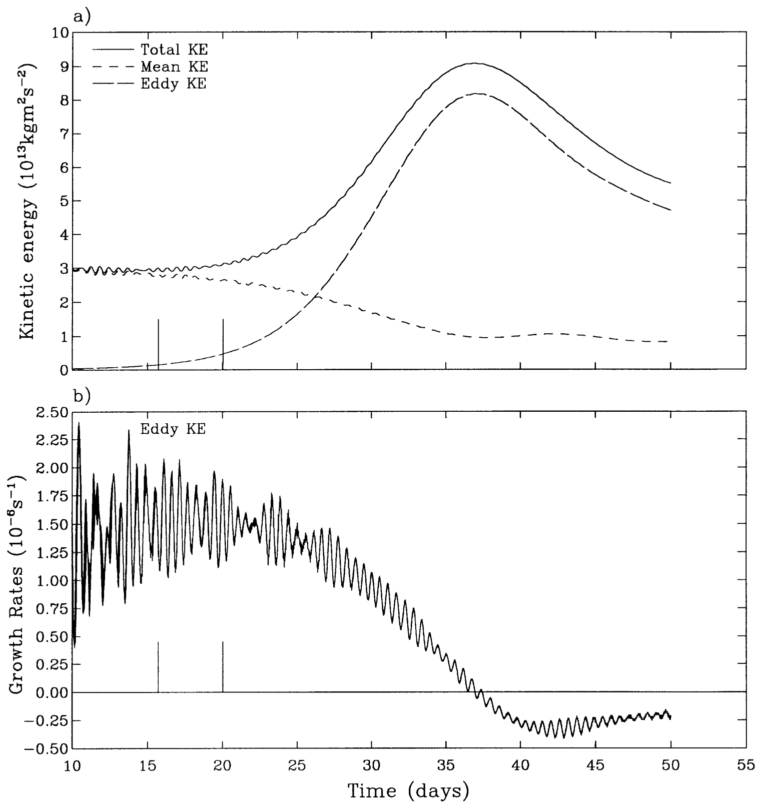

Fig. 4. A time series of (a) the total, mean and eddy kinetic energy, and (b) the growth rates, from the 133 km length flat-channel run with the BB model, initialized with the subsurface front. The 2 vertical lines in the time series mark the time period over which the growth rates are averaged for the growth rate curve.

the disturbance is time-independent*. These are called normal mode solutions; their temporal and spatial dependence can be expressed as independent factors of the general solution. When normal modes grow exponentially during the early stages of instability, the growth rates are steady (see formula above). So steady growth rates, in each model run, correspond to a time during which exponential normal mode growth occurs. It is during this time that the instabilities in the model are the numerical counterparts of the normal mode solutions found by a linear stability analysis of the QG equations. Since this time period is different for each model run, we averaged the growth rates of the velocity field (as defined above) over the period when the ratio of KE'/KE is between 5% and 15%, in order to obtain objective growth rate curves for each experiment.

* This is the case with linear QG theory.

Fig. 4a shows a time series of KE, $\overline{KE}$, and KE' from a 50-day run with the BB model ("FCT" version) for a channel length of 133 km. A time series of the growth rates as defined by the formula above, is shown in Fig. 4b. The vertical bars on the time series show the time period over which the growth rates were averaged, for the case shown. The high frequency oscillations seen in Fig. 4b are inertial oscillations in the model. As can be seen from Fig. 4a, these oscillations are small, as the initial fields are in geostrophic balance. (It is because the growth rate values are such a sensitive parameter that their presence is so evident in Fig. 4b.) The meander starts to extract kinetic energy from the front at day 15, thereby reducing the mean kinetic energy, $\overline{KE}$.

(These graphs indicate the rate of change of $\overline{KE}$ and KE', but not the dynamic processes by which these changes occur.) Subsequently, the growth rate remains fairly constant, indicative of exponential growth. As the wave grows, dissipation plays a larger rôle and the growth rate values decay. As expected, when the eddy kinetic energy, KE', peaks at day 35 the growth rate becomes negative.

Having determined the linear growth rate for a certain channel length, the length of the channel and the initial perturbation were varied, and again the growth rate was noted. In this way, growth rate could be plotted against wavenumber. These growth rate curves provide a succinct way of summarizing the early stages of the meander development.

For the parameters appropriate to the model setup, QG theory predicts a maximum linear growth rate of $2.08 \times 10^{-6}\,\mathrm{s}^{-1}$ ($0.180\,\mathrm{day}^{-1}$) to occur at an along-channel wavelength of 125.7 km (see Section 7). With no explicit friction or diffusion, the numerical QG model reproduces this maximum well. The QG model was run with Laplacian friction using a viscosity coefficient of $5 \times 10^5\,\mathrm{cm}^2\,\mathrm{s}^{-1}$ (the same value used for lateral viscosity coefficients in the BC and BB models) to assess the effect of viscosity on these results. Fig. 5 shows the growth rate curves from the QG model with and without viscosity. The magnitude of the growth rates is reduced by 11%, and the fastest growing wave occurs at a slightly longer wavelength, when viscosity is introduced. This wavenumber shift is to be expected, since Laplacian friction is more effective in damping the shorter waves. The 11% reduction in the magnitude of the growth rates simple means that viscosity slows down the growth of individual baroclinic waves. The consequences of this in a realistic oceanic modelling scenario will depend on the type of waves excited and on the non-linear interaction between these waves. Subsequent runs incorporating topography into the QG model are performed with no viscosity or diffusion, in order to produce accurate growth rate curves.

As mentioned in Subsection 2.2, two versions of the BB model were run. Fig. 6 shows the growth rate curves from these 2 versions of the code: "centred" and "FCT". Both versions have isopycnal viscosity and no explicit density diffusion. This figure nicely illustrates how the FCT scheme has a dampening effect on the waves. This is achieved by the presence of implicit diffusion in the thickness equation. The wavelength of the fastest growing wave remains the same in these 2 runs, indicating that the diffusion is independent of wave number. This may not be the case for all scenarios, since the diffusion in the FCT scheme is dependent on the horizontal density gradients.

Eulerian discretization of the non-linear advection terms is a non trivial numerical problem.

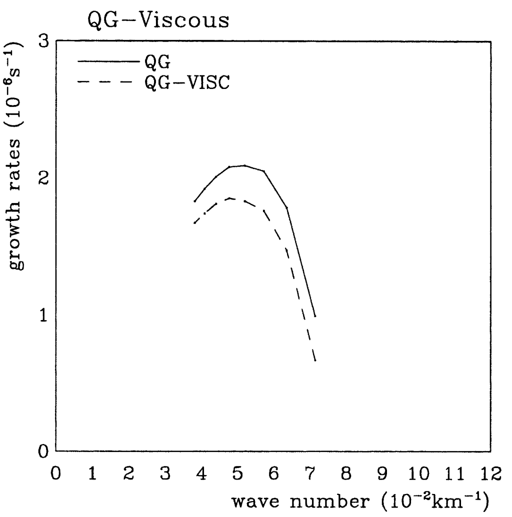

Fig. 5. Growth rate curves from the QG model with and without viscosity.

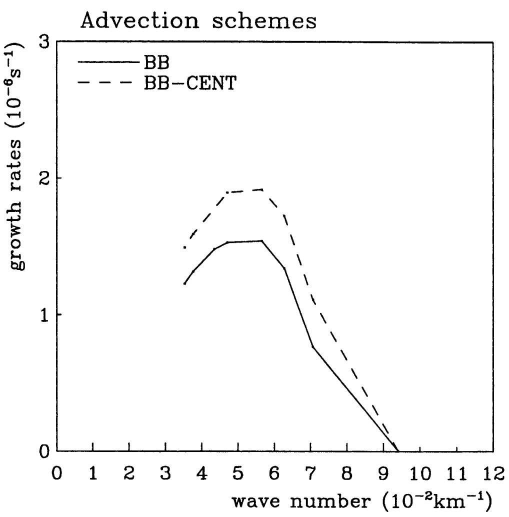

Fig. 6. Growth rate curves from the "centred" and the "FCT" versions of the BB model.

Numerically efficient schemes either smooth out (dissipate) anomalies as they are advected along, or disperse anomalies, by decomposing a portion of the original distribution into a combination of short waves or ripples. Excessive dispersion is undesirable, since physical inconsistencies can arise when the advected quantity must remain positive definite (e.g., salinity, thickness of an isopycnal layer). On the other hand, numerical dissipation can smooth out strong gradients to such a degree that interesting dynamical features get blurred (e.g., salt pockets, steep fronts). Dissipation errors can frequently be written mathematically as a diffusive term (i.e., a discrete form of $\partial^2/\partial x^2$), and can therefore be thought of as implicit diffusion. The FCT numerical scheme uses both a dispersive high-order scheme and a diffusive low-order scheme. The 2 are combined using an "anti-diffusive flux", which is constrained such that new maxima and minima are not introduced by the numerical scheme itself (i.e., to restrict dispersion). This constraint, which is dependent on the horizontal density gradients in the fluid, determines the rôle of diffusion and dispersion occurring due to the scheme. Although the scheme is designed to minimize dispersion, it may introduce some numerical diffusion (Rood, 1987). This implicit diffusion weakens the large-scale horizontal density gradients thereby reducing the baroclinic growth rates.

Notice that the magnitude of the maximum growth rate in the "centred" version of the BB model lies between that found in the two QG runs (with and without Laplacian friction). Figs. 5, 6 illustrate how both viscosity and diffusion dampen the growth rate of baroclinic waves. The largest maximum growth rates are found in the QG model with no viscosity and no diffusion ($2.13 \times 10^{-6}\,s^{-1} = 0.184$ day^{-1}); followed by the "centred" version of the BB model ($1.99 \times 10^{-6}\,s^{-1} = 0.172$ day^{-1}) and the QG model with viscosity ($1.85 \times 0^{-6}\,s^{-1} = 0.160$ day^{-1}), which both have viscosity but no diffusion; with the smallest maximum growth rates found in the "FCT" version of the BB model ($1.59 \times 10^{-6}\,s^{-1} = 0.137$ day^{-1}), which has explicit viscosity and significant implicit diffusion. All subsequent experiments with the BB model are performed with the "FCT" version because of its ability to incorporate topography.

The stability curves from the QG model and the 2 primitive equation models (BC and "FCT" version of BB) in a flat-bottomed channel are shown in Fig. 7. Both primitive equation models have lower growth rate magnitudes than the QG model. This is because of the presence of viscosity and diffusion in these models, as discussed above. Notice that the maximum growth rate value in the BC model lies between that found by the QG model with viscosity (Fig. 5) and the BB model. The diffusion implicit in the FCT scheme employed by the BB model suppresses the instabilities more than the explicit diffusion in the BC model. We deduce that, in a flat-bottomed channel, the BC model has a more active baroclinic eddy field than the BB model, in response to the same potential energy field. A series of experiments were performed with the BC model, varying the channel length, in which both the horizontal viscosity and diffusion coefficients were doubled. This resulted in a 17.5% reduction in the maximum growth rate value and a slight shift to smaller wavenumbers, producing a growth rate curve similar to the "FCT" version of the BB model. This simply affirms the conclusions drawn above, about the effects of viscosity and diffusion on baroclinic growth rates.

The growth rate curves approach their maxima very gradually, which makes it difficult to determine the exact wavelength of the fastest growing

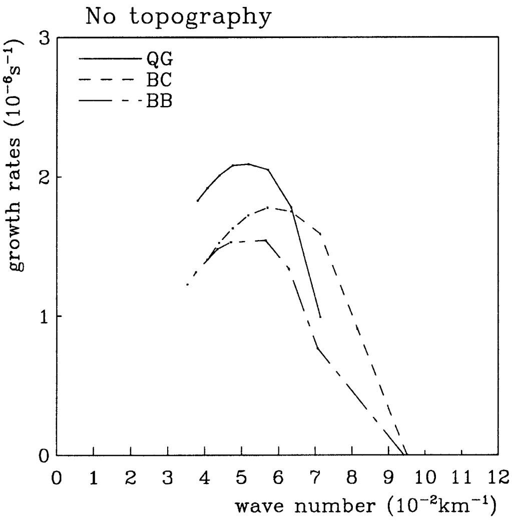

Fig. 7. Growth rate curves for the flat-channel runs in all 3 models.

Table 1. *Wavelengths of the fastest growing baroclinic wave along the subsurface front in a flat channel*

Model	Wavelength of fastest growing wave	Wavelength range having growth rates $\geqslant 95\%$ of maxima
QG	118 km	107–130 km
BC	105 km	92–118 km
BB	120 km	109–134 km

wave. In fact, the range of wavelengths for which growth rates are $\geqslant 95\%$ of the maxima, is ~ 25 km. This range and the estimated wavelength of the fastest growing mode for the QG, BC, and BB models are shown in Table 1.

Notice that the fastest growing wave in the BC model is some 13 km shorter than that found by the QG model. In these experiments, carefully designed to reproduce quasi-geostrophic baroclinic instability, this is a defect of the BC model which does not occur in the BB model. Since the physics of the BB and BC models are the same, we investigate numerical reasons for this feature. The 3 primary differences between these 2 models are:

(i) the BC model has explicit Laplacian diffusion whilst the BB model has implicit diffusion introduced by the FCT scheme;

(ii) the BC model employs the Arakawa B-grid whilst the BB model uses the Arakawa C-grid;

(iii) vertical discretization results in the thermodynamic variables being defined at the same fixed level as the dynamic variables in the BC model, whilst in the BB layer model each isopycnal layer has a constant density value and variable thickness.

The consequences of these 3 differences will now be discussed sequentially.

Laplacian diffusion in the BC model is more effective at dissipating smaller waves. Its presence in the BC model will therefore act to move the growth rate maximum to smaller wavenumbers (larger wavelengths). This is not the tendency that is observed. We can therefore conclude that diffusion in the BC model is not responsible for shifting the growth rate maximum in the BC model to higher wavenumbers. In addition, comparison of the growth rates for the 2 versions of the BB model ("centred" and "FCT") suggests that the implicit diffusion inherent in the FCT scheme affects the magnitude of the growth rates equally for all wavelengths.

Numerical analysis and experiments (Arakawa and Lamb, 1977; Wajsowicz, 1986) indicate that the Arakawa B-grid is best for coarse resolution simulations, whilst the Arakawa C-grid is to be preferred for finer resolution simulations. However, the degree to which this may be an issue in different oceanographic simulations is unclear. Both grids have their disadvantages: the B-grid requiring interpolation for the pressure gradient terms, and the C-grid requiring interpolation for the Coriolis terms. In order to estimate the errors associated with the horizontal discretization, experiments were performed with the BC model, in which the horizontal resolution was doubled (i.e., Δx was halved). If the B-grid is responsible for the shift in wavenumber space of the growth rate peak, the increased resolution run would reduce this tendency. However, the only change seen in the growth rate curves was a marginal increase (5%) in the growth rates values, but no wavenumber shift.

The wavenumber shift found in the BC model can be explained by the vertical discretization chosen. Ikeda and Wood (1993) found the stability properties of primitive equation models to be dependent on the vertical discretization. When the continuous equations are discretized such that the thermodynamic variables (i.e., density and pressure) are defined at the same level as the dynamic variables (i.e., u and v), the fastest growing mode is shifted to shorter wavelengths unless the vertical resolution is extremely fine. The BC model is of this type and will therefore exhibit these tendencies. The vertical resolution in this model might be considered to be reasonable: 6 layers in the upper 200 m, which is where the perturbation is found. However, Wood and Ikeda (1994) found that very high resolution was needed in the BC model (minimally 10 m thickness levels in the upper 90 m) in order to produce a growth rate curve similar to the reference solution (a QG model simulation). This explains why the BC model shifts the maximum growth rate to higher wavenumbers.

3.3. *Positive topographic slope*

Topography is now introduced to the channel, such that the topographic slope is in the same

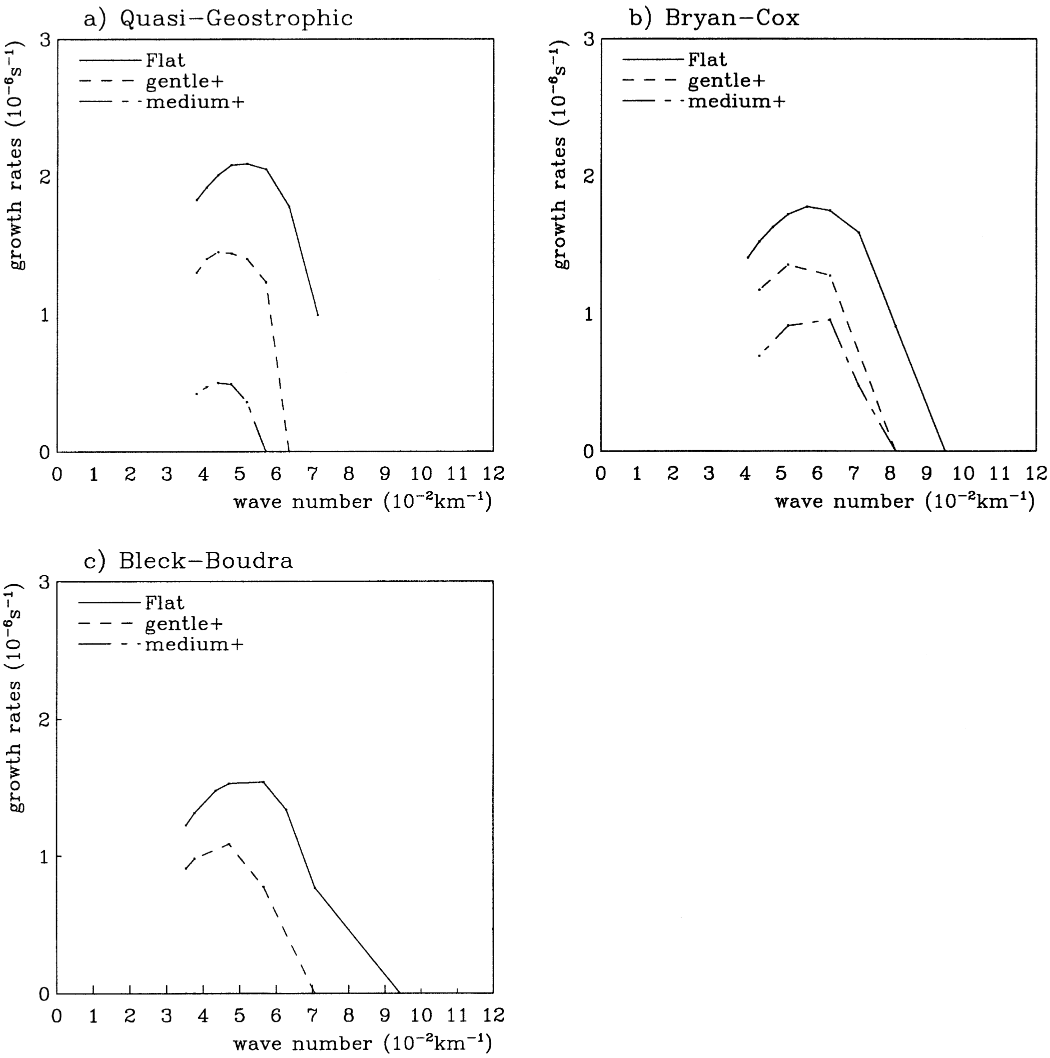

Fig. 8. Growth rate curves with no topography, and with gentle and medium positive topographic slope, for (a) the QG model, (b) the BC model, and (c) the BB model.

direction as the frontal slope. This is referred to as a positive topographic slope. The topography varies across the channel only. This alignment mimics a coastal current flowing parallel to a continental shelf; e.g., the Florida current. The magnitude of the slope is progressively increased, choosing values of: 1.5×10^{-3}, 2.5×10^{-3}, and 5×10^{-3}. These slopes will be referred to as "gentle", "medium", and "steep", respectively. As the slope is introduced, the maximum depth of the channel is increased such that the water depth in the centre of the channel (where the front is found) remains 1000 m. In the BC model, this meant that the number of layers in the model had to be increased to 21, 22 and 25 layers respectively. Only the "FCT" version of the BB model was run for the topographic cases since the "centred" version of the model was not designed to cope with sloping bottoms. The steep slope case (5×10^{-3}) was not run for the QG model, as this was considered to be beyond its capability (given the QG assumptions).

These runs with the subsurface front can be compared with the analytical results, provided the topographic slope isn't so steep that the QG approximation becomes invalid. QG theory tells us that a positive slope will reduce the growth rates and increase the wavelength of maximum growth (see Section 7). This effect becomes more pronounced as the topographic slope is increased.

Baroclinic waves grew in the presence of positive bottom slope topography, with an energy cycle similar to that found in the flat-channel cases. Fig. 8a–c show the growth rate curves for the QG, BC, and BB models respectively, for the flat-bottomed case and the 3 runs with positive topography. Both primitive equation models exhibit the same basic trend: a stabilization of the waves and a slight shift of the maxima to smaller wavenumbers, this effect increasing with the topographic slope. Since this behaviour was predicted by QG theory, and reproduced by the QG model, we can say that both primitive equation models cope with this kind of topographic configuration well.

In both primitive equation models, no waves grew in the presence of the steep slope. Extrapolation of the QG results (both theoretical and the numerical, cf. Fig. 8a) indicates that such a slope is sufficient to suppress wave growth, for the baroclinicity of the front under consideration here. For the medium slope case of 2.5×10^{-3}, no waves grew in the BB model, whilst baroclinic instability was simulated in both the QG and BC models. As discussed in Subsection 3.2, implicit diffusion associated with the FCT scheme is responsible for repressed eddy activity in the BB model. We conclude that the BC model will have the most active eddy field when a topographic slope of this orientation is significant, and that the growth of baroclinic waves is sensitive to not only the magnitude of diffusion, but also to the numerical discretization of the thermodynamic equation (both advection and diffusion terms).

Fig. 9 shows the stability curves for the positive gentle slope, 1.5×10^{-3}, in the 3 different models. The maximum in the BC model occurs at a higher wavenumber than the QG model, whose maximum has a slightly higher wavenumber than the BB model. This wavenumber discrepancy between the BC and QG models was observed in the flat-bottomed case and can be attributed to the vertical discretization in the BC model. The wave number shift of the maximum growth rate in the BC model, due to both the gentle and medium bottom slope, is less than that found in both the BB and QG models. This suggests that the wave number errors in the BC model due to the vertical discretization, are exacerbated in a more stable environment. Subsequent experiments with negative topographic slope (see below) confirm this conclusion.

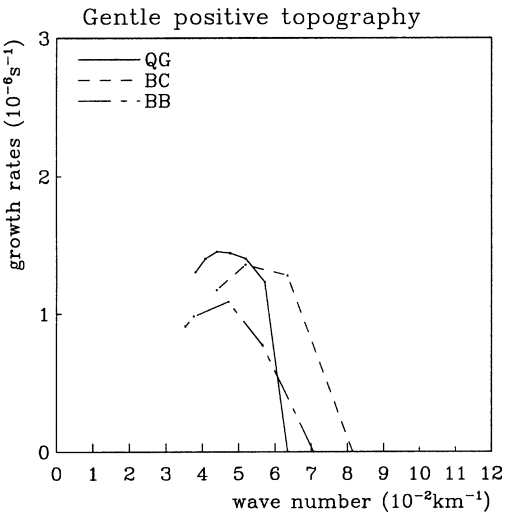

Fig. 9. Growth rate curves for the positive gentle slope in all 3 models.

3.4. *Negative topographic slope*

Topography is now introduced which slopes in the opposite direction to the frontal slope. We refer to this as a negative topographic slope. Such a configuration is liable to behave quite differently than the positive topographic slope case, since the movement of potential vorticity is inhibited by both isopycnals and the sea bed (cf. Fig. 1). Again, the magnitude of the slope is progressively increased, using gentle, medium, and steep slopes.

QG theory predicts a shift of the maximum growth rate to higher wavenumbers and a marginal increase in the growth rate values, when negative topography is introduced. As the topographic slope is increased further, the shift to higher wavenumbers persists, but the maximum growth rate value falls slightly below that of the flat-bottomed case. The point at which the maximum growth rate value starts to decrease depends

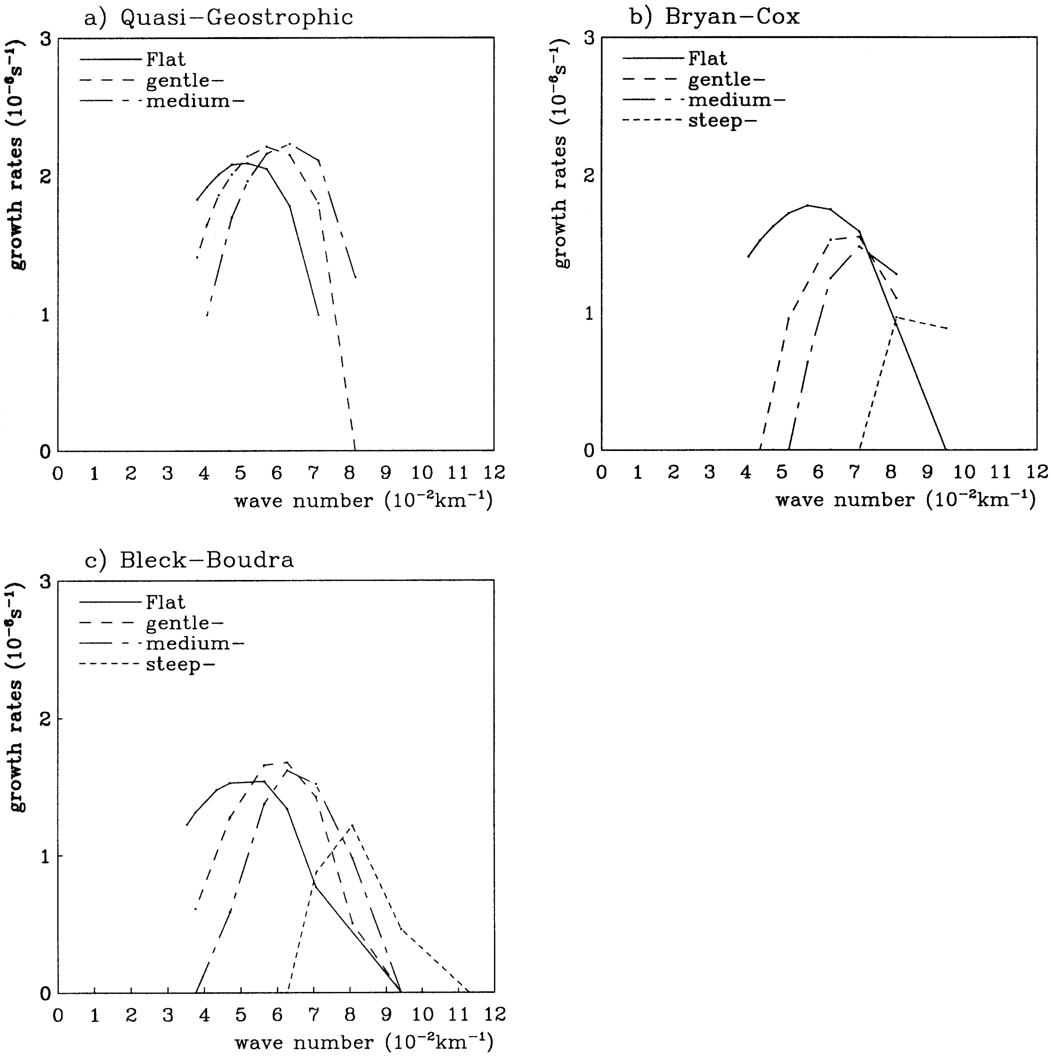

Fig. 10. Growth rate curves with no topography and with gentle, medium, and steep negative topographic slope, for (a) the QG model, (b) the BC model, and (c) the BB model.

on the across-channel structure of the wave. The smaller the across-channel wavenumber, the sooner the waves are damped as progressively steeper negative topography is introduced (see Section 7). However, negative topography does not reduce the QG growth rates to the same degree that positive topography does, whatever the meridional structure of the waves.

Chao's (1990) numerical results of a coastal current simulation, forced by a buoyancy flux, found this orientation of topography to be more stabilizing than the positive topography. He investigated the instability of outcropping fronts in the presence of a continental shelf which had a slope of 3.75×10^{-3}. These conditions did not satisfy the quasi-geostrophic assumptions. His criterion for determining instability was based on observations of a fully developed meander: either a meander developed or it didn't. As Chao points out, when considering ageostrophic fronts, which orientation of topography will enhance or suppress baroclinic instability should be answered on a case by case basis.

Fig. 10a–c show the stability curves for the negative topography runs, for the QG, BC, and BB models respectively. (Again the steep slope run was omitted for the QG model.) All the models progressively move the maximum growth rate to higher wavenumbers as steeper negative topography is introduced, in agreement with QG baroclinic instability theory (described above). The shift in wavelength is similar for all 3 models. Both primitive equation models develop baroclinic waves with steep negative topography, in contrast to the steep positive topography experiments.

The introduction of negative topography has quite different consequences on the magnitudes of the growth rates in the 2 primitive equation models. The growth rates in the BC model are reduced with gentle and medium bottom slope, whilst for the BB model the magnitude of the maximum growth rate remains the same. The waves are damped more in the BC model than the BB model with negative topographic slope. (The converse was found in the experiments with positive topographic slope.) The reason for this is explained in the next paragraph.

Fig. 11 shows the stability curves for the gentle negative slope, for the 3 models. Both primitive equation models have significantly smaller growth rates than the QG model, which simply reflects the absence of diffusion and viscosity in the QG model. The viscosity and diffusion in the BC and BB models, although they behave quite differently, both act to suppress the instabilities. The growth rates of the BC model are slightly smaller than those in the BB model, in contrast to the positive topographic case. In this case (with negative bottom slope), when the background field is highly unstable, the implicit diffusion in the BB model is minimal. We can deduce that the dissipation in the BB model weakens the frontal gradient the most (thereby suppressing baroclinic instability) when the background field is weakly unstable. One might have expected this behaviour, since the FCT scheme was designed with the purpose of advecting steep gradients well, but tends to fracture smoother anomalies into a series of shock fronts (Rood 1987).

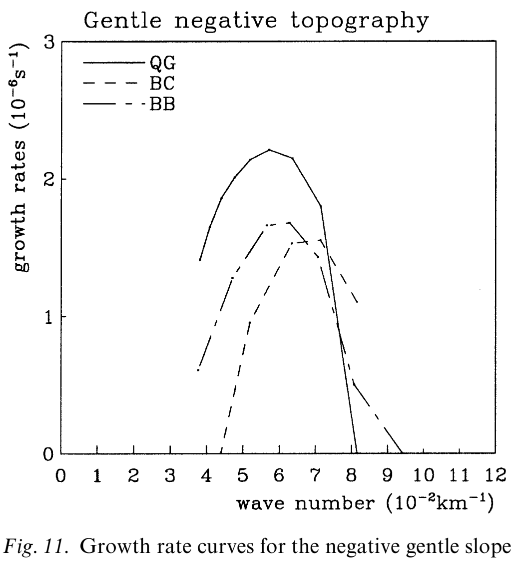

Fig. 11. Growth rate curves for the negative gentle slope in all 3 models.

4. Ageostrophic, outcropping front instabilities

In this section, we investigate the stability properties of an ageostrophic, outcropping front in the 2 primitive equation models. The physical characteristics of the channel described in Subsection 2.3 remain unchanged. Two thermodynamic profiles* were used to define a cold fresh water mass and a warm salty water mass, the division of which forms the basis of the front. These profiles were chosen to be representative of the coastal waters and the open ocean off the Labrador coast. A linear transition between these 2 water masses was made over a 20 km distance in the centre of the channel. In the BC model, 20 levels were used to describe the vertical structure for the flat channel, using the same thicknesses as was used for the subsurface front (see Section 3). In the BB model, 13 isopycnal layers were used, with an interval of 0.1 σ_T units. The vertical structure of the isopycnals is shown in Fig. 12. Minima (i.e., large negative values) in the initial potential vorticity correspond to the regions of strongest stratification: in the near surface layers at one side of the channel, and between 200 m and 300 m on the other side of the channel. The maximum velocity associated with this front is 106.9 cm s^{-1}.

* Temperature and salinity for the BC model, and isopycnal thickness for the BB model.

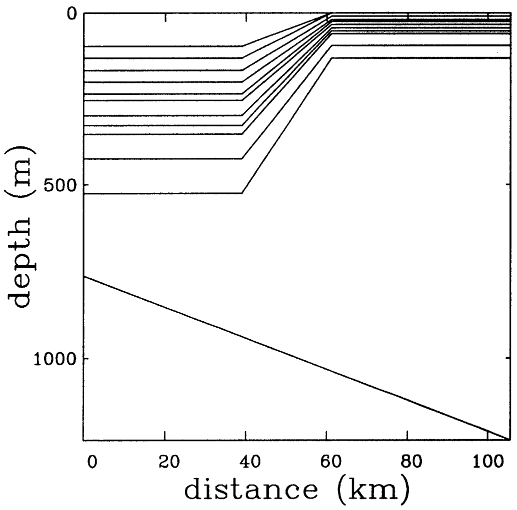

Fig. 12. Across-channel section of the initial density field with steep negative topography in the BB model. Contour interval is 0.1 σ_T units.

We approach this investigation in a similar manner to that used for the subsurface front in Section 3. First we determine the stability properties of the front with no topography, and then introduce progressively steeper topography. With the outcropping front, we only investigate the negative topography scenario, since this is the orientation of the bottom topography off the Labrador coast. For instabilities along an ageostrophic front with positive topography (e.g., like the Florida current), another choice of stratification would be more appropriate. In these experiments the initial front does not intersect the bottom slope topography, as is the case off the Labrador coast. We remind the reader of our primary aim, which is to monitor the performance of the numerical models as we gradually introduce more realistic scenarios, not to attempt to simulate a realistic scenario. However, we hope that this paper will inspire more numerical studies which will broaden the application of these results.

In order to draw the stability curves for this type of front, we used the trick of varying the channel length in order to simulate the growth of different wavelengths. We determine the growth rates for varying channel lengths: (i) with no topography, (ii) with gentle negative topography, and (iii) with steep negative topography. (Here we have used the same slopes to define gentle and steep topography as was used in Subsection 3.3) Again for the gentle and steep topography in the BC model, the number of levels was increased to 21 and 25 respectively, so that the water depth beneath the front remained 1000 m.

For the experiments with a flat channel the BB model took 5 × as long to run as the BC model. However, when topography was introduced, the BC model was only 3 × as fast as the BB code.

4.1. *Growth of baroclinic normal modes*

The models were initialized by imposing a sinusoidal perturbation in the upper 220 m on the outcropping front, and using the corresponding geostrophic velocities for the dynamic fields. The models were run for several weeks, as before, and time series of eddy kinetic energy and growth rate were plotted in order to determine the linear growth rate. However, no periods of constant growth rate were found, indicating that normal mode exponential growth was not occurring. Not only is this undesirable for comparing model growth rates, since we could be comparing the growth of 2 quite different waves; but the absence of a period with steady growth rates, makes it difficult (if not impossible) to determine a growth rate representative of the linear stages of instability. Since the vertical structure of this front is considerably more complicated than the subsurface front discussed in Section 3 (which could simply be regarded as 2 water masses), the initial perturbation which was given to the model may not have been a normal mode solution of this front. If it had been, it would have had a time-independent structure as exponential growth occurred. When we examined the vertical structure of the waves, the shape was seen to change during the initial growth. Several experiments were performed changing the vertical structure of the initial perturbation, but the normal modes were never found. Thus we decided not to perturb the front initially, but to allow the models to choose the structure of the most unstable wave. With this approach, an instability developed (after some time) which proved to be a normal mode with a steady growth rate period. Consequently a linear growth rate value could be determined quite easily. Again we varied the channel lengths to simulate the growth of a variety of wavelengths. Analysis of the energetics of these waves showed that they were all baroclinic waves, extracting potential energy from the mean horizontal density gradients and converting it into eddy kinetic energy.

4.2. Experiments in a flat channel and with negative topography

Figs. 13, 14 show the growth rate curves for the BC and BB models respectively, with no initial perturbation. In each figure, 3 curves are shown for the cases with no topography, with gentle negative topography, and with steep negative topography. As expected, the growth rate values in the flat channel are much larger with the outcropping front than for the subsurface front, since the density gradients are stronger. No sensible comparison between the magnitude of these growth rates and those found with the subsurface front can be made unless a measure of the baroclinicity of the front is taken into account (i.e., the

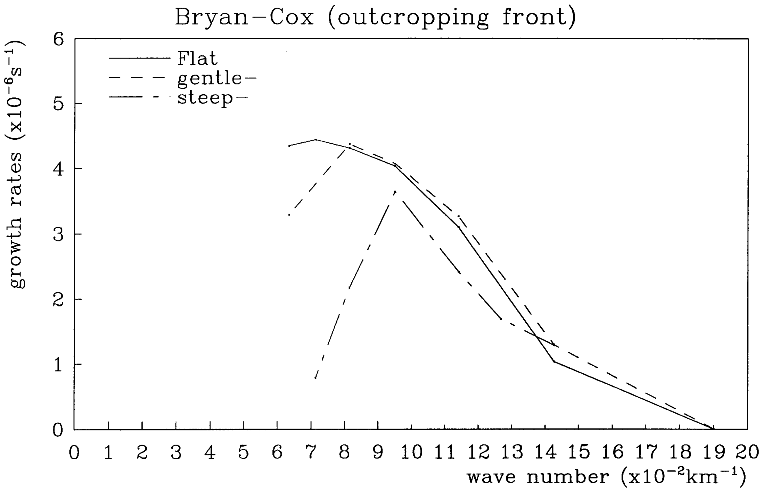

Fig. 13. The growth rate curves for flat, gentle negative, and steep negative topography, in the BC model initialized with the outcropping front.

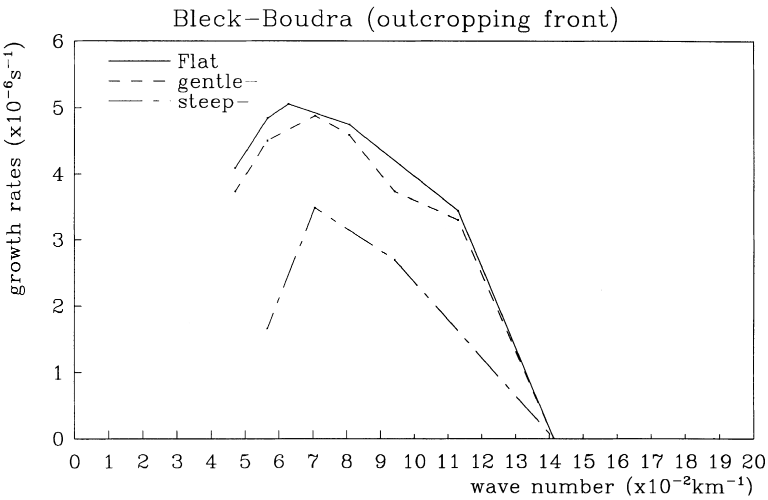

Fig. 14. The growth rate curves for flat, gentle negative, and steep negative topography, in the BB model initialized with the outcropping front.

strength of the density gradients, or equivalently the strength of the current). This can be done by normalizing the growth rates by the maximum velocities associated with the fronts. The normalized maximum growth rates for the flat-channel experiments are: $5.68 \times 10^{-6}\,\mathrm{m}^{-1}$ and $5.47 \times 10^{-6}\,\mathrm{m}^{-1}$ for the subsurface front; and $4.41 \times 10^{-6}\,\mathrm{m}^{-1}$ and $5.01 \times 10^{-6}\,\mathrm{m}^{-1}$ for the outcropping front, in the BC and BB models respectively. So ageostrophic effects act to stabilize baroclinic waves in these 2 models. This is in agreement with previous studies (Derome and Dolph, 1970; Wood and Ikeda, 1994). In response to the outcropping front in a flat channel, the BB model has somewhat higher growth rates than the BC model, in contrast to the growth rates found with the subsurface front. This reinforces the deduction made at the end of Subsection 3.4; that is, diffusion in the BB model becomes minimal in highly unstable situations (i.e., strong baroclinicity).

The fastest growing wave in the flat channel is 95 km in the BB model, and 82 km in the BC model. A similar discrepancy was observed with the subsurface front. This feature simply illustrates one of the consequences of the vertical discretization used by the BC model: that is, to shift the maximum growth rate to higher wavenumbers. The short wave instability cut-off in the BB model occurs at a longer wavelength than in the BC model. Although this feature is of secondary importance to any discrepancies in the maxima of the growth rate curves, it is worthy of note since baroclinic waves having smaller growth rates will manifest in an oceanic simulation given the appropriate forcing.

When topography is introduced the growth rate maxima shift to shorter wavelengths; and with steep enough slope, the waves grow much slower. This trend is similar to that found in the subsurface front experiments. We deduce that the effects of negative topography in a quasi-geostrophic context can be extrapolated into ageostrophic environments. In their numerical experiments with an even steeper front (a stratification based on the Iceland-Faerœ front) Maskell et al. (1992) also found such a trend. The shift to smaller wavelengths of the fastest growing wave is more pronounced in the BC model when the steep slope is introduced. In both models, the magnitudes of the growth rates are significantly reduced only in the presence of the steep slope. We notice again, that as the conditions progress to a more stable situation (by the introduction of steeper negative topography), the BB model has a smaller maximum growth rate than the BC model. This can be attributed to the implicit diffusion in the BB model as discussed in Subsection 3.4.

5. Conclusions

In this study of baroclinic instability, we have demonstrated that numerically induced errors are present during the linear stage of growth in both the primitive equation models used. When interpreting the results of numerical models, wise oceanographers will not assume that stable solutions are free from numerical errors. All primitive equation models will produce solutions with some kind of numerical error. The important concern is that the errors are not too large, and that modellers are aware of the types of numerical error which their particular model is predisposed to.

Computational resources are often a consideration for the large oceanographic models in use today. The "FCT" version of the BB model needed 7× as much CPU time to run the model with 2 isopycnal layers, in a flat channel, compared with the "centred" version. The BC model was the most computationally efficient of the primitive equation models, despite needing more levels to resolve the topography and density structure, in all the experiments we performed.

The existence of viscosity and diffusion in the models, regardless of the manner in which they operate (isopycnal or otherwise), reduces the initial growth rate of the baroclinic waves. In flat-channel runs with the BB model, using the subsurface front as a basic state, the "FCT" version of the model produced much smaller growth rates (19% smaller) than the "centred" version of the model. This comparison between 2 versions of the BB model code simply demonstrates that implicit diffusion, inherent in the FCT scheme, can be significant. In fact, in these experiments, the implicit diffusion in the "FCT" version of the BB model reduces the baroclinic growth rate more than the BC model does with a diffusion coefficient of $5 \times 10^5\,\mathrm{cm}^2\,\mathrm{s}^{-1}$. The magnitude of the diffusion in the scheme will vary according to the topography and the baroclinicity of the front. It may be that in the non-linear stage, the character of such waves is modified by the type of viscosity and diffusion that is employed (Drijfhout 1992). We have not investigated this aspect for reasons discussed in the introduction, choosing to focus on the linear growth stage of the waves which could be validated.

In both the subsurface and outcropping front experiments, the fastest growing baroclinic wave was significantly shorter in the BC model than that in the BB model. The comparison with QG results (theoretical and numerical) for the subsurface front in Subsection 3.3 reveals that this is a defect of the BC model. This feature can be understood by theoretical work (Ikeda and Wood, 1993) which demonstrates that it is the vertical discretization used by the BC model which is responsible for moving the baroclinic growth rate curve to higher wavenumbers. Numerical modellers ought to be aware that this model will naturally (that is, in the absence of topographic or external forcing) produce baroclinic waves which have too short a wavelength. This will have repercussions on the non-linear interactions between growing waves. Indeed, retarded growth rates, due to numerical diffusion (discussed in the preceeding paragraph) will also affect non-linear interactions. Exactly how this may affect the resulting flow field must be investigated in each particular scenario. This complex topic is beyond the scope of this paper.

Baroclinic instability along the (geostrophic) subsurface front in both primitive equation models is modified by topographic slopes (both positive and negative) in the manner expected from QG theory and numerical QG model results. This result will be reassuring to numerical modellers using these 2 models, particularly where topographically modified baroclinic waves are an important feature. The fastest growing wave becomes longer and is dampened when positive topography is introduced, and becomes shorter when negative topography is introduced. The same trend is observed in response to the (ageostrophic) outcropping front overlying a negative slope, in both primitive equation models. Thus, ageostrophy does not change the way that topography modifies the baroclinic growth rates, at least in the linear stages of growth. Normalized growth rate magnitudes along the subsurface front were compared with those found along the ageostrophic outcropping front. In both models ageostrophic effects act to dampen the waves, in agreement with theory (Derome and Dolph, 1970).

In response to the subsurface front, the BC model has faster growing baroclinic waves than the "FCT" version of the BB model, both in a flat channel and with positive topographic slope. However, the converse is true when a negative topographic slope is introduced, and for the outcropping front experiments, both in a flat channel and with gentle negative slope. These results suggest that the diffusion associated with the FCT scheme is most active in weak baroclinically unstable environments.

Numerical models in use today invariably produce stable and physically realistic flow fields. This can easily lead to a false sense of confidence in numerical results, which is compounded by the lack of verifying data. The results presented here demonstrate how physically realistic baroclinic waves in numerical models may not replicate the dynamics of the real ocean, because of numerical errors which can modify the wave characteristics. Interpretation of numerical results will be more accurate and more useful to the oceanographic community, when numerical modellers are aware of the types of errors that can arise. The work presented here contributes to this important aspect of numerical modelling.

We summarize by emphasizing 2 numerical characteristics of the models used in this study. Firstly, maximum baroclinic growth rate occurs at too short a wavelength in the BC model, because of the vertical discretization used. This will also be a tendency in other models which use the same type of vertical discretization (Ikeda and Wood, 1993). In contrast, the BB layer model accurately reproduces the wavelength of the fastest growing wave. Secondly, numerical modellers using FCT schemes ought to be aware of the rather unpredictable nature of diffusion inherent in the scheme, particularly in realistic simulations. The diffusion associated with this scheme can be quite large or insignificant, depending on the likelihood of baroclinic instability. This may or may not be physically realistic and ought to be investigated for each application.

6. Acknowledgements

Catherine Griffiths would like to acknowledge the support of a Canadian government NSERC fellowship and the hospitality of Dr Stephen Maskell and the mathematics department at Exeter University. Motoyoshi Ikeda appreciated the support of the Scientific Research, Japanese Ministry of Education, Science, Sports and Culture.

7. Appendix

For completeness, the dispersion relation for a QG 2-layer fluid with topography is derived. The governing equations (cf. Pedlosky 1979, Subsection 6.16) for the upper and lower layers respectively are:

$$\frac{\mathrm{d}}{\mathrm{d}t_1}[\nabla^2 p_1 + F_1(p_2 - p_1)] = -\beta \frac{\partial p_1}{\partial x}, \tag{A.1}$$

$$\frac{\mathrm{d}}{\mathrm{d}t_2}\left[\nabla^2 p_2 + F_2(p_1 - p_2) + \frac{f_\mathrm{o}^2}{H_2} h_\mathrm{B}\right] = -\beta \frac{\partial p_2}{\partial x}, \tag{A.2}$$

where p_i is the dynamic pressure in the ith layer; $\mathrm{d}/\mathrm{d}t_i = \partial/\partial t + u_i\, \partial/\partial x + v_i\, \partial/\partial y$; (u_i, v_i) are the geostrophic velocities in the ith layer; $F_i = f_\mathrm{o}^2/g'H_i$, H_i is the thickness of the ith layer; g' is the reduced gravity; and h_B is the height of the topography. In order to derive these equations, we have used the Boussinesq and geostrophic approximations, and assumed that interface variations and topographic variations are small compared with the layer depth. The QG assumption remains valid provided the time scale characteristic of the motions is much longer than one day. (This is certainly the case for baroclinic waves in the ocean.)

Now we assume that $h_\mathrm{B} = h_\mathrm{B}(y)$, and define a purely baroclinic mean flow such that $u_1 = \bar{U}$, and $u_2 = 0$. Then the pressure field associated with this mean flow is: $p_1 = -f_\mathrm{o}\bar{U}y$, and $p_2 = 0$. Linearizing the equations about this mean state, we have:

$$\left(\frac{\partial}{\partial t} + \bar{U}\frac{\partial}{\partial x}\right)[\nabla^2 p_1 + F_1(p_2 - p_1)] + F_1\bar{U}\frac{\partial p_1}{\partial x} = -\beta\frac{\partial p_1}{\partial x}, \tag{A.3}$$

$$\frac{\partial}{\partial t}[\nabla^2 p_2 + F_2(p_1 - p_2)] + \frac{f_\mathrm{o}}{H_2}\frac{\partial p_2}{\partial x}\frac{\partial h_\mathrm{B}}{\partial y} - F_2\bar{U}\frac{\partial p_2}{\partial x} = -\beta\frac{\partial p_2}{\partial x}. \tag{A.4}$$

Assuming normal mode solutions of the form

$$p_i = \mathrm{Re}\{A_i \mathrm{e}^{i(kx + ly - \omega t)}\}, \tag{A.5}$$

and substituting into the governing equations, we have:

$$[k(\beta + F_1\bar{U}) + (\omega - \bar{U}k)(k^2 + l^2 + F_1)]A_1 + (\bar{U}k - \omega)F_1 A_2 = 0, \tag{A.6}$$

$$-\omega F_2 A_1 + \left[k\left(\beta - F_2\bar{U} + \frac{f_\mathrm{o}}{H_2}\frac{\partial h_\mathrm{B}}{\partial y}\right) + (k^2 + l^2 + F_2)\omega\right]A_2 = 0. \tag{A.7}$$

These 2 equations can be written in matrix form. For non-trival solutions, p_i, the determinant of this 2-dimensional matrix must be zero. Hence,

$$\omega^2(\phi_1\phi_2 - F_1F_2) + \omega k\left\{\phi_1\left(\beta - F_2\bar{U} + \frac{f_\mathrm{o}}{H_2}\frac{\partial h_\mathrm{B}}{\partial y}\right) + \phi_2(\beta + F_1\bar{U}) - \bar{U}(\phi_1\phi_2 - F_1F_2)\right\} + k^2(\beta + F_1\bar{U} - \bar{U}\phi_1)\left(\beta - F_2\bar{U} + \frac{f_\mathrm{o}}{H_2}\frac{\partial h_\mathrm{B}}{\partial y}\right) = 0, \tag{A.8}$$

where $\phi_i = k^2 + l^2 + F_i$. This is the dispersion relation for baroclinic waves in a 2-layer fluid in the presence of topography.

For the subsurface front described in Section 3, the appropriate parameters for the dispersion relation are: $H_1 = 200$ m, $H_2 = 800$ m, $\bar{U} = 0.169\ \mathrm{ms}^{-1}$, $\rho_1 = 1026.6926\ \mathrm{kg\ m}^{-3}$, $\rho_2 = 1027.7495\ \mathrm{kg\ m}^{-3}$, $f_\mathrm{o} = 1.1914 \times 10^{-4}\ \mathrm{s}^{-1}$, $\beta = 1.3094 \times 10^{-11}\ \mathrm{m}^{-1}\ \mathrm{s}^{-1}$ and $l = 200$ km. (l was chosen to correspond to a wavelength equal to twice the channel width.)

REFERENCES

Arakawa, A. and Lamb, V. R. 1977. Computational design of the basic dynamical processes of the UCLA general circulation model. In: *Methods in computational physics* **17**, Academic Press, pp. 174–264.

Asselin, R. 1972. Frequency filter for time integrations. *Mon. Wea. Rev.* **100**, 487–490.

Bleck, R. and Boudra, D. B. 1981. Initial testing of a numerical ocean circulation model using a hybrid (quasi-isopycnic) vertical coordinate. *J. Phys. Oceanogr.* **11**, 755–770.

Bleck, R. and Boudra, D. B. 1986. Wind-driven spin-up in eddy-resolving ocean models formulated in isopycnic and isobaric coordinates. *J. Geophys. Res.* **91**, 7611–7621.

Bleck, R. and Smith, L. 1990. A wind-driven isopycnic coordinate model of the north and equatorial Atlantic Ocean. Part I: Model development and supporting experiments. *J. Geophys. Res.* **95**, 3272–3285.

Bryan, K. 1969. A numerical method for the study of the circulation of the world ocean. *J. Comp. Phys.* **4**, 347–376.

Chao, S. 1990. Instabilities of fronts over a continental margin. *J. Geophys. Res.* **95**, 3199–3211.

Chassignet, E. P. 1992. Rings in numerical models of ocean general circulation—a statistical study. *J. Geophys. Res.* **97**, 9479–9492.

Cox, M. D. 1984. *A primitive equation, 3-dimensional model of the ocean*. GFDL Ocean Group Tech. Report, No. 1, 250 pp.

Cox, M. D. and Bryan, K. 1984. A numerical model of the ventilated thermocline. *J. Phys. Oceanogr.* **14**, 674–687.

Derome, J. and Dolph, C. L. 1970. Three-dimensional non-geostrophic disturbances in a baroclinic zonal flow. *Geophys. Fluid Dyn.* **1**, 91–122.

Drijfhout, S. S. 1992. Ring genesis and the related heat transport. Part II: A model comparison. *J. Phys. Oceanogr.* **22**, 268–285.

Fofonoff, N. P. 1962. Physical properties of sea water. *The Sea*, Vol. 1. New York, Interscience, 864 pp.

Griffiths, C. 1992. Modelling the Iceland Faerœ front. PhD thesis, Univ. of Exeter, Exeter, England. 191 pp.

Hecht, M. W., Holland, W. R. and Rasch, P. J. 1995. Upwind-weighted advection schemes for ocean tracer transport—an evaluation in a passive tracer context. *J. Geophys. Res.* **100**, 20,763–20,778.

Hecht, M. W., Bryan, F. O. and Holland, W. R. 1998. A consideration of tracer advection schemes in a primitive equation ocean model. *J. Geophys. Res.* **103**, 3301–3321.

Hoskins, B. and Bretherton, F. P. 1972. Atmospheric frontogenesis models: mathematical formulation and solution. *J. Atmos. Sci.* **29**, 11–37.

Huppert, H. E. and Bryan, K. 1976. Topographically generated eddies. *Deep Sea Res.* **23**, 655–679.

Ikeda, M. 1981. Meanders and detached eddies of a strong eastward-flowing jet using a two-layer quasi-geostrophic model. *J. Phys. Oceanogr.* **11**, 526–540.

Ikeda, M. and Wood, R. A. 1993. Mesoscale stability of an ocean current in the Bryan–Cox model. *J. Geophys. Res.* **98**, 12,527–12,536.

Killworth, P. D. 1987. Topographic instabilities in level model OGCMs. *Ocean Modelling* **75**.

Killworth, P. D., Stainforth, D., Webb, D. J. and Paterson, S. M. 1991. The development of a free-surface Bryan–Cox–Semtner ocean model. *J. Phys. Oceanogr.* **21**, 1333–1348.

Lazier, J. R. N. and Wright, D. G. 1993. Annual velocity variations in the Labrador Sea. *J. Phys. Oceanogr.* **23**, 659–678.

LeBlond, P.H. 1982. Satellite observations of Labrador Current undulations. *Atmosphere–Ocean* **20**, 129–142.

Lorenz, E. 1967. *The nature and theory of the general circulation of the atmosphere*. World Meteorol. Organization, Geneva.

Matsuno, T. 1966. Numerical integrations of the primitive equations by a simulated backward difference method. *J. Meteor. Soc. Japan* **44**, 76–84.

Maskell, S. J., Heathershaw, A. D. and Stretch, C. E. 1992. Topographic and eddy effects in a primitive equation model of the Iceland–Faeroes front. *J. Marine Systems* **3**, 343–380.

New, A. L., Bleck, R., Jia, Y., Marsh, R., Huddleston, M. and Barnard, S. 1995. An isopycnic model study of the north Atlantic. Part I: Model experiment. *J. Phys. Oceanogr.* **25**, 2667–2699.

Oberhuber, J. 1993. Simulation of the Atlantic circulation with a coupled sea ice-mixed layer-isopycnal general circulation model. Part I: Model description. *J. Phys. Oceanogr.* **23**, 808–829.

Orlanski, I. and Cox, M. D. 1973. Baroclinic instability in ocean currents. *Geophys. Fluid Dyn.* **3**, 297–332.

Pedlosky, J. 1979. *Geophysical fluid dynamics*. Springer-Verlag, 624 pp.

Roberts, M. J., Marsh, R., New, A. L. and Wood, R. A. 1996. An intercomparison of a Bryan–Cox-type ocean model and an isopycnic ocean model. Part I: The subpolar gyre and high-latitude processes. *J. Phys. Oceanogr.* **26**, 1495–1527.

Rood, R. B. 1987. Numerical advection algorithms and their rôle in atmospheric transport and chemistry models. *Reviews of Geophys.* **25**, 71–100.

Smith, L. T. 1992. Numerical simulations of stratified rotating flow over finite amplitude topography. *J. Phys. Oceanogr.* **22**, 686–696.

Wajsowicz, R. C. 1986. Free planetary waves in finite-difference numerical models. *J. Phys. Oceanogr.* **16**, 773–789.

Wang, W. 1997. The gulf stream near 73°W: views from observations and a primitive equation model. *Deep Sea Research, Part I. Oceanographic Research Papers*, **44**, 1147–1166.

Wilkin, J. L., Mansbridge, J. V. and Godfrey, J. S. 1995. Pacific ocean heat transport at 24°N in a high-resolution global model. *J. Phys. Oceanogr.* **25**, 2204–2214.

Wood, R. A. and Ikeda, M. 1994. Comparison of mesoscale meanders and eddies simulated by quasigeostrophic and primitive equation models: a case study. *J. Geophys. Res.* **99**, 22,645–22,663.

Zalesak, S. T. 1979. Fully multidimensional flux-corrected transport algorithms for fluids. *J. Comp. Phys.* **31**, 335–362.